Gross-Pitaevskii equation for Bose particles in a double-well potential: Two-mode models and beyond

D. Ananikian and T. Bergeman
Department of Physics and Astronomy, SUNY, Stony Brook, New York 11794-3800, USA
(Received 28 March 2005; revised manuscript received 31 August 2005; published 5 January 2006)

In this work, our primary goal has been to explore the range of validity of two-mode models for Bose-Einstein condensates in double-well potentials. Our derivation, like others, uses symmetric and antisymmetric condensate basis functions for the Gross-Pitaevskii equation. In what we call an "improved two-mode model" (I2M), the tunneling coupling energy explicitly includes a nonlinear interaction term, which has been given previously in the literature but not widely appreciated. We show that when the atom number (and hence the extent of the wave function) in each well vary appreciably with time, the nonlinear interaction term produces a temporal change in the tunneling energy or rate, which has not previously been considered to our knowledge. In addition, we obtain a parameter, labeled "interaction tunneling," that produces a decrease of the tunneling energy when the wave functions in the two wells overlap to some extent. Especially for larger values of the nonlinear interaction term, results from this model produce better agreement with numerical solutions of the time-dependent Gross-Pitaevskii equation in one and three dimensions, as compared with models that have no interaction term in the tunneling energy. The usefulness of this model is demonstrated by good agreement with recent experimental results for the tunneling oscillation frequency [Albiez *et al.*, Phys. Rev. Lett. **95**, 010402 (2005)]. We also present equations and results for a multimode approach, and use the I2M model to obtain modified equations for the second-quantized version of the Bose-Einstein double-well problem.

DOI: 10.1103/PhysRevA.73.013604 PACS number(s): 03.75.Lm, 05.45.−a, 03.75.Kk

I. INTRODUCTION

The analogy between double Bose-Einstein condensates, separated by a barrier, and Josephson oscillations of superconductors [1] was apparently first suggested by Javanainen [2], and has been developed more thoroughly in a number of theoretical studies [3–20]. Especially from work in [4,5,10] and more recently in [12,18], a rather elaborate picture of phase-space dynamics has now been developed. The equations for tunneling oscillations of Bose-Einstein condensates in a double-well potential have been shown to resemble a pendulum whose length depends on the momentum. In the limit of small-amplitude oscillations, the equations are the same as for Josephson oscillations for superconductors separated by a weak link [21]. It has also been shown that when atom-atom interactions exceed a critical value, the ensemble will remain trapped in one well while the phase continually increases, resembling a pendulum with sufficient energy to rotate.

Experiments showing interference when condensates in a potential with a barrier were released [22] first stimulated interest in the problem of Bose-Einstein condensates in a double-well potential. More pertinent to the present discussion are experiments that probe the evolution of the distribution between two or more wells of an optical lattice. Josephson oscillations have been observed in one-dimensional (1D) optical potential arrays [23]. Recently for a double-well potential, both the regimes of tunneling and self-trapping of Rb atoms were observed [24]. In view of proposed extensions of these and other experimental techniques [25–29], it seems appropriate now to reexamine the theory with the goal of developing models to deal with more diverse conditions.

It is often assumed that the "tight-binding" approximation is valid, leading to what is known as the Bose-Hubbard model [30,31], or discrete nonlinear Schrödinger equation [32,33]. This model, which has been confirmed under the experimental conditions of [23], employs parameters for tunneling and on-site energy that are usually taken to be constant. One expects that with sufficiently large numbers of atoms, the atom-atom repulsion will cause the wave functions in a well to vary in size depending on the atom number, and consequently, the tunneling parameter and on-site energy might vary.

In this paper, we show that solutions of a two-mode model based on symmetric and antisymmetric solutions of the Gross-Pitaevskii equation [11,13,20,34], yield a parametrization for the double-well problem that produces agreement with solutions of the time-dependent Gross-Pitaevskii equation up to large values of the interaction term. Applied in 3D to actual experiments on Bose-Einstein condensates in a double-well potential [24], this parametrization reproduces the oscillation frequencies within experimental error, while a simpler model exhibits self-trapping behavior under the same conditions. The key element here is a tunneling parameter that explicitly includes interaction effects. Although similar tunneling parameters have been presented in the past by Giovanazzi *et al.* [13], the implications have not been examined in detail. We will refer to this more exact two-mode model as an "improved two-mode" (I2M) model, to distinguish it from the standard two-mode (S2M) model, in which an interaction term does not appear in the expression for the tunneling parameter. Despite the additional terms needed for the I2M, the equations eventually reduce to the same form as for the S2M or for the usual Bose-Josephson junction equations. However, the parameters are defined differently, and there is one additional term that can be significant for strong interactions and high barriers.

Below, we compare results obtained with the I2M to those obtained with the S2M, with results of a multimode model, and then with numerical solutions of the time-dependent Gross-Pitaevskii equation (TDGPE). The parameters used in the two- or multimode models are obtained from numerical solution of the stationary Gross-Pitaevskii (GP) equation, so it is perhaps not surprising that the model that mimics the GP equation most closely also best reproduces results from the TDGPE. For very large interactions, results from any two-mode model will deviate from the TDGPE results, but agreement is most persistent with the I2M. Under conditions of a particular experiment, effects of nonzero temperature and experimental uncertainties may be larger than the differences shown below.

The present study emphasizes a mean-field approach using the GP equation, assumes that fluctuations and thermal excitations are negligible, and does not quantize particle number. Thus the particle number difference and phase difference of atoms in two wells or two modes are classical quantities in this approach. Considerable theoretical effort has been devoted to second-quantized forms [4,7–9,18,19]. We show in Sec. II E that the I2M leads to a second-quantized model containing terms that can be interpreted as correlated hopping effects. As shown in Ref. [18], the classical patterns appear clearly in the quantum phase-space picture with as few as ten atoms.

An outline of this paper is as follows. Section II is devoted to 1D models. After a brief presentation of the time-dependent Gross-Pitaevskii equation for double-well problems (Sec. II A), we present equations for two-mode models and compare certain results (Sec. II B). Sec. II C lays out a multimode approach, Sec. II D discusses dynamics in phase space, and Sec. II E gives equations for a second-quantized version. Experiments are of course in 3D, with some degree of transverse confinement. Therefore in Sec. III we present a formalism for 3D calculations and give a few results, including comparisons with the experimental results of Ref. [24].

II. MODELS

A. Time-dependent Gross-Pitaevskii equation

When the temperature is sufficiently low and when particle numbers are sufficient that second-quantization effects are not important, the time-dependent Gross-Pitaevskii equation may be used for the wave function $\psi(x,t)$ for interacting Bose-Einstein condensate atoms at zero temperature in an external potential $V_{\rm ext}(x)$. Letting $\hbar=m=1$, a dimensionless version is

$$i\frac{\partial\psi}{\partial t}=-\frac{1}{2}\frac{\partial^2\psi}{\partial x^2}+V_{\rm ext}\psi+g|\psi|^2\psi. \tag{1}$$

The relationship between g and g_{3D} will be discussed in Sec. III A. Here $\int dx\,|\psi(x,t)|^2=N$, where N is the number of atoms. Except in Sec. II E, N is not quantized, and the approach is strictly mean field.

We consider double-well potentials $V_{\rm ext}(x)$ that are symmetric in x. Initially, we discuss one-dimensional versions. Under the above conditions, we will use results obtained with the TDGPE to test two-mode and multimode models discussed below. The TDGPE can tell us, for example, whether the phase is nearly constant as a function of x over an individual well.

B. Two-mode models

In many situations, a good approximation is obtained with a two-mode representation of $\psi(x,t)$. In early work [4], wave functions localized in each well were used. Later, ± combinations of symmetric and antisymmetric functions, as in Refs. [5,10,11] provided a more accurate formulation, and we follow the approach of Ref. [11] here:

$$\psi(x,t)=\sqrt{N}[\psi_1(t)\Phi_1(x)+\psi_2(t)\Phi_2(x)], \tag{2}$$

$$\Phi_{1,2}(x)=\frac{\Phi_+(x)\pm\Phi_-(x)}{\sqrt{2}}, \tag{3}$$

where

$$\Phi_\pm(x)=\pm\Phi_\pm(-x),\quad \int dx\,\Phi_i\Phi_j=\delta_{i,j},\quad i,j=+,-. \tag{4}$$

The $\Phi_\pm$ will be assumed to be real, and to satisfy the stationary GP equations

$$\beta_\pm\Phi_\pm=-\frac{1}{2}\frac{d^2\Phi_\pm}{dx^2}+V_{\rm ext}\Phi_\pm+\bar{g}|\Phi_\pm|^2\Phi_\pm, \tag{5}$$

with $\bar{g}=gN$.

We can now define

$$z(t)\equiv|\psi_1(t)|^2-|\psi_2(t)|^2, \tag{6}$$

$$\phi(t)\equiv\theta_2(t)-\theta_1(t). \tag{7}$$

Here $\theta_i(t)$ are the phase arguments of the complex-valued function $\psi_i(t)$: $\psi_i(t)=|\psi_i(t)|e^{i\theta_i(t)}$. The above normalization conventions lead to a constraint on the $\psi_i(t)$:

$$\int_{-\infty}^{\infty}dx|\psi|^2=N\Rightarrow|\psi_1(t)|^2+|\psi_2(t)|^2=1. \tag{8}$$

Note that Φ_1 (Φ_2) primarily occupies the left (right) well, but has nonzero density on the other side. In order to compare with results of the TDGPE, we define the number of atoms in the left well as follows:

$$N_L=\int_{-\infty}^{0}dx|\psi(x,t)|^2=\frac{N}{2}+NzS, \tag{9}$$

and we define S and Δn as

$$S=\int_{-\infty}^{0}dx\,\Phi_+(x)|\Phi_-(x)|,\quad \Delta n=\frac{N_L-N_R}{N}=2zS. \tag{10}$$

From the ansatz (2), the TDGPE (1), and the GP equation (5), eventually one obtains differential equations for z and ϕ. We here briefly outline this derivation. In the following, these quantities will be used:

$$\gamma_{ij} = \bar{g} \int \Phi_i^2(x)\Phi_j^2(x)dx \quad (i,j = +,-),$$

$$\Delta\gamma = \gamma_{--} - \gamma_{++},$$

$$\Delta\beta = \beta_- - \beta_+,$$

$$A = \frac{10\gamma_{+-} - \gamma_{++} - \gamma_{--}}{4},$$

$$B = \beta_- - \beta_+ + \frac{\gamma_{++} - \gamma_{--}}{2} = \Delta\beta - \frac{\Delta\gamma}{2},$$

$$C = \frac{\gamma_{++} + \gamma_{--} - 2\gamma_{+-}}{4},$$

$$F = \frac{\beta_+ + \beta_-}{2} - \gamma_{+-}, \tag{11}$$

where β_+ and β_- are defined in Eq. (5). Substitution of Eqs. (2) and (5) into Eq. (1) yields

$$i\frac{d\psi_1(t)}{dt}(\Phi_+ + \Phi_-) + i\frac{d\psi_2(t)}{dt}(\Phi_+ - \Phi_-) = \sum_{\pm}\left[(\psi_1(t) \pm \psi_2(t)](\beta_\pm - gN|\Phi_\pm|^2)\Phi_\pm + \frac{gN}{2}\sum_{\pm}(\Phi_\pm^3 P_\pm + \Phi_\pm^2\Phi_\mp Q_\pm)\right], \tag{12}$$

where

$$P_\pm = 2(\psi_1 \pm \psi_2) - |\psi_1|^2\psi_1 \mp |\psi_2|^2\psi_2 \pm \psi_1^2\psi_2^* + \psi_2^2\psi_1^*,$$

$$Q_\pm = \pm 2(\psi_2 - \psi_1) + 5\psi_1|\psi_1|^2 \mp 5\psi_2|\psi_2|^2 \pm \psi_1^2\psi_2^* - \psi_2^2\psi_1^*.$$

The usefulness of the $\Phi_\pm$ basis is evident here, since integrals with odd powers of Φ_+ or Φ_- vanish. From the above equations, the following equations for $\dot{\psi}_{1,2}(t)$ are obtained for the I2M:

$$i\frac{d\psi_1}{dt} = \left(F + A|\psi_1|^2 - \frac{\Delta\gamma}{4}\psi_1\psi_2^*\right)\psi_1 - \left(\frac{\Delta\beta}{2} - \frac{\Delta\gamma}{4}|\psi_2|^2 - C\psi_1^*\psi_2\right)\psi_2 = \mathcal{M}_1\psi_1 - \mathcal{K}_1\psi_2,$$

$$i\frac{d\psi_2}{dt} = \left(F + A|\psi_2|^2 - \frac{\Delta\gamma}{4}\psi_2\psi_1^*\right)\psi_2 - \left(\frac{\Delta\beta}{2} - \frac{\Delta\gamma}{4}|\psi_1|^2 - C\psi_2^*\psi_1\right)\psi_1 = \mathcal{M}_2\psi_2 - \mathcal{K}_2\psi_1. \tag{13}$$

By contrast, evolution equations for the S2M are written typically as follows:

$$i\frac{d\psi_1}{dt} = (E_1^0 + U_1|\psi_1|^2)\psi_1 - \mathcal{K}\psi_2,$$

$$i\frac{d\psi_2}{dt} = (E_2^0 + U_2|\psi_2|^2)\psi_2 - \mathcal{K}\psi_1, \tag{14}$$

where, for $i=1$ or 2,

$$E_i^0 = \int dx\left(\frac{1}{2}|\nabla\Phi_i|^2 + |\Phi_i|^2 V_{\text{ext}}\right),$$

$$U_i = gN\int dx|\Phi_i|^4,$$

$$\mathcal{K} = -\int dx\left(\frac{1}{2}(\nabla\Phi_1\,\nabla\,\Phi_2) + \Phi_1 V_{\text{ext}}\Phi_2\right). \tag{15}$$

To relate E_i^0 $(i=1,2)$ to $\beta_\pm$ and $\gamma_{\pm,\pm}$, we define, for $i = +,-$,

$$\epsilon_i = \int dx\left(-\frac{1}{2}\Phi_i\frac{d^2\Phi_i}{dx^2} + \Phi_i V_{\text{ext}}\Phi_i\right) = \beta_i - \bar{g}\langle|\Phi_i|^4\rangle = \beta_i - \gamma_{ii}. \tag{16}$$

Then

$$E_1^0 = E_2^0 = E = \frac{\epsilon_+ + \epsilon_-}{2}. \tag{17}$$

Furthermore,

$$U_1 = U_2 = U = \bar{g}\langle|\Phi_{1,2}|^4\rangle = \frac{\bar{g}}{4}\langle|\Phi_+ \pm \Phi_-|^4\rangle = \frac{1}{4}(\gamma_{++} + 6\gamma_{+-} + \gamma_{--}) = A + 2C. \tag{18}$$

In the symmetric or antisymmetric basis, the coupling term becomes

$$\mathcal{K} = \frac{\epsilon_- - \epsilon_+}{2} = \frac{\Delta\beta - \Delta\gamma}{2} = \frac{B}{2} - \frac{\Delta\gamma}{4}. \tag{19}$$

Comparison of Eqs. (13) and (14), and definitions of quantities therein, tells us the essential differences in the two models. In the S2M, the tunneling parameter $\mathcal{K}$ does not explicitly involve atom-atom interactions, and does not vary when z and ϕ vary. To understand the effective tunneling parameter(s) in the I2M, we need $|\psi_{1,2}|^2 = (1\pm z)/2$ and $\psi_1^*\psi_2 = (1/2)\sqrt{(1-z^2)}e^{i\phi}$. Thus in the limit $z=\phi=0$, the effective I2M tunneling parameters are

$$\mathcal{K}_1 = \mathcal{K}_2 = \frac{\Delta\beta}{2} - \frac{\Delta\gamma}{8} + \frac{C}{2} = \mathcal{K} + \frac{3\Delta\gamma}{8} + \frac{C}{2}. \tag{20}$$

The magnitude of this difference between $\mathcal{K}_{1,2}(z=\phi=0)$ and $\mathcal{K}$ will be shown below for various cases.

For $z>0, \phi=0$, $\mathcal{K}_1$ increases in value and $\mathcal{K}_2$ decreases, while the reverse is the case for $z<0, \phi=0$. As more atoms accumulate on the left side, the wave function expands due

to the repulsive atom-atom interaction, so the tunneling rate to the right increases. At the same time, the wave function on the right diminishes and the tunneling from right to left decreases, as expected. We find that this effect is typically smaller than the correction to $\mathcal{K}_i$ for $z=0$ discussed above.

The term in C is an even smaller effect. To understand the role of C, it is helpful to rewrite it as

$$C = \bar{g} \int dx\, \Phi_1^2 \Phi_2^2, \tag{21}$$

which shows that C increases as the overlap of the right and left wave functions increases. This occurs when β_+ approaches the top of the barrier, near the limit of validity of any two-mode model, as discussed below. Under such circumstances, and when $\phi=0$, $|z|$ is maximum, the term in C produces a decrease in both $\mathcal{K}_1$ and $\mathcal{K}_2$. This is therefore a "pre-tunneling" effect proportional to the nonlinear interaction that we will refer to as "interaction tunneling." When the wave functions are already overlapped to some extent, the tunneling capability is diminished by an amount that depends on the interaction.

Remarkably, despite some complexity of the additional terms in the I2M, relatively simple equations of familiar form can be obtained with no approximations beyond the assumption of a two-mode representation of ψ, as in Eq. (2). Equations (1), (2), (5), (12), and (3) are used. We obtain for the I2M

$$\frac{d\phi}{dt} = Az + \frac{Bz}{\sqrt{1-z^2}} \cos\phi - Cz \cos 2\phi,$$

$$\frac{dz}{dt} = -B\sqrt{1-z^2} \sin\phi + C(1-z^2)\sin 2\phi. \tag{22}$$

These equations can be written in Hamiltonian form,

$$\dot{z} = -\frac{\partial H}{\partial \phi}, \quad \dot{\phi} = \frac{\partial H}{\partial z} \tag{23}$$

with the Hamiltonian

$$H_{\mathrm{I2M}} = A\frac{z^2}{2} - B\sqrt{1-z^2}\cos\phi + \frac{1}{2}C(1-z^2)\cos 2\phi. \tag{24}$$

This Hamiltonian is an integral of motion for a classical system with generalized coordinates $(z(t), \phi(t))$ and dynamical properties (22) and will be referred to later as a classical Hamiltonian. H is not equal to the expectation value $\langle\psi\mathcal{H}\psi\rangle/\langle\psi\psi\rangle$ of the quantum Hamiltonian $\mathcal{H} = -\frac{1}{2}\partial^2/\partial x + V_{\mathrm{ext}}(x) + g|\psi|^2$ within the two-mode approximation (2). Since $\psi(x,t)$ defined as Eq. (2) is not an eigenfunction of $\mathcal{H}$, the expectation value $\langle\psi\mathcal{H}\psi\rangle/\langle\psi\psi\rangle$ is not constant over time. However, the Hamiltonian (24) provides information about dynamics in phase space, including self-trapping, as will be discussed in Sec. II D.

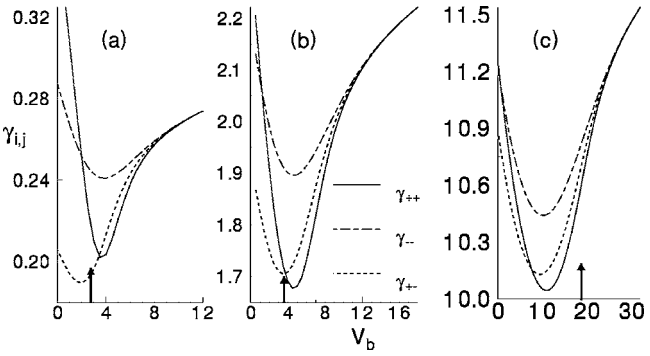

FIG. 1. Parameters $\gamma_{++}, \gamma_{--}, \gamma_{+-}$ as a function of V_b for $gN = 1.0$ (a), 10.0 (b), and 100.0 (c), calculated using the DVR method applied to the stationary GP equation (5). The vertical arrows denote values of V_b for which $\beta_+ = V_b$. All quantities plotted in this and all other figures are dimensionless, with scalings as given after Eq. (28).

For the S2M, the corresponding Hamiltonian is

$$H_{\mathrm{S2M}} = U\frac{z^2}{2} - 2\mathcal{K}\sqrt{1-z^2}\cos\phi. \tag{25}$$

In the limit $|z| \ll 1$, the Josephson-junction form is

$$H_{\mathrm{S2M}} \approx E_c\frac{z^2}{2} - E_J\cos\phi, \tag{26}$$

where E_c is the on-site Coulomb energy and E_J is the Josephson coupling energy. Thus $A \approx E_c \approx U$ and $B \approx E_J \approx 2\mathcal{K}$. We note here that the expression given in Ref. [13] for E_J can be shown to be identical to B:

$$E_J = -N\int dx\, \Phi_1(x)[H_0 + gN\Phi_1^2(x)]\Phi_2(x) = B \tag{27}$$

where $H_0 = -(1/2)d^2/dx^2 + V_{\mathrm{ext}}(x)$.

Having outlined these two two-mode models, we now consider the range of parameters, to give estimates of the magnitude of various effects. In numerical work we often used a harmonic potential with Gaussian barrier of varying height and width:

$$V_{\mathrm{ext}}(x) = \frac{1}{2}x^2 + V_b e^{-(x/\sigma)^2}. \tag{28}$$

Equations (2) and (5) imply that distances are scaled by $\alpha_x = \sqrt{\hbar/M\omega_x}$, time by $1/\omega_x$ and energies, including V_b above, by $\hbar\omega_x$, where M is the atomic mass, and $\omega_x/2\pi$ is the harmonic frequency. This scaling will be used throughout this paper, and in particular in all the figures. To obtain numerical values for the overlap integrals γ_{ij}, where $i,j=\pm$, we solved Eq. (5) using the discrete variable representation (DVR) method [35,36] with increasingly finer mesh, with iterations for each mesh to make the $\Phi_\pm$ functions and the nonlinear term self-consistent. Values for the γ_{ij} are shown as a function of barrier height V_b for $\sigma=1.5$, for $gN=1, 10$, and 100, in Fig. 1. For large enough V_b, all parameters γ_{ij} are equal. As V_b decreases from the asymptotic region, γ_{++} decreases

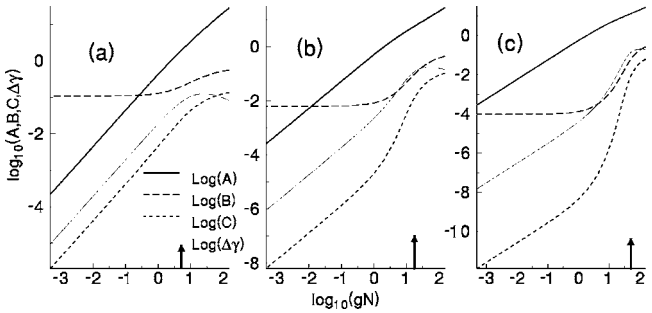

FIG. 2. A, B, C, and $\Delta\gamma$ parameters as a function of $\bar{g}=gN$, on a log-log scale. The three plots are for $\sigma=1.5$, and $V_b=4.0$ (a), 7.0 (b), and 12.0 (c) in units of $\hbar\omega_z$. The vertical arrows denote values of $\log \bar{g}$ for which $\beta_+=V_b$.

most rapidly because Φ_+, with no node, is less "lumpy" than Φ_-.

A useful estimate for the condition for a two-mode model to be valid is that $\beta_+ \leqslant V_b$ [33]. With this rough criterion in mind, in many of the plots, we will denote this point by vertical arrows. By this test, in Fig. 1, two-mode models are valid to the right of the arrows, while in Fig. 2, the regime of validity of two-mode models is to the left of the arrows. In reality, the transition is not sharp, as we will see below.

In Fig. 2, values for the parameters A, B, C, and $\Delta\gamma$ are shown. A, the on-site energy, increases roughly linearly with $\bar{g}$. B is constant for small and moderate $\bar{g}$, which is consistent with the usual expression for E_J or $\mathcal{K}$ which omits an interaction term. As β_+ approaches V_b (as indicated by the arrows) B begins to increase, and C and $\Delta\gamma$ increase more rapidly. The parameter C (the "interaction tunneling" parameter) is several orders of magnitude smaller than A, B, and $\Delta\gamma$ except when $\bar{g}$ is large compared to 1. When C is much smaller than $\Delta\gamma$, it is justified to neglect C but preserve the difference between B and $\Delta\beta$. When $\bar{g}$ is sufficiently large, the C term may become significant, although we have found that within the regime of validity of two-mode models, the ratio C/B is never greater than 0.15. We emphasize that the term comes strictly from the nonlinear Gross-Pitaevskii equation for Bose-Einstein condensates in a double-well potential and does not apply to superconducting Josephson junctions.

The two two-mode models may be compared, for example, on the predictions for the plasma oscillation frequency [15], which is taken to be the oscillation frequency in the limit of small amplitudes of z and ϕ. In the limit of small z and ϕ, the equations for $\dot{z}$ and $\dot{\phi}$ become

$$\frac{dz}{dt} = -2\mathcal{K}\phi, \quad \frac{d\phi}{dt} = (U+2\mathcal{K})z$$

$$\Rightarrow \omega_{0S}^2 = 2\mathcal{K}(U+2\mathcal{K}) \quad \text{(S2M)}$$

$$\frac{dz}{dt} = (2C-B)\phi, \quad \frac{d\phi}{dt} = (A+B-C)z$$

$$\Rightarrow \omega_{0I}^2 = (B-2C)(A+B-C) \quad \text{(I2M)}. \qquad (29)$$

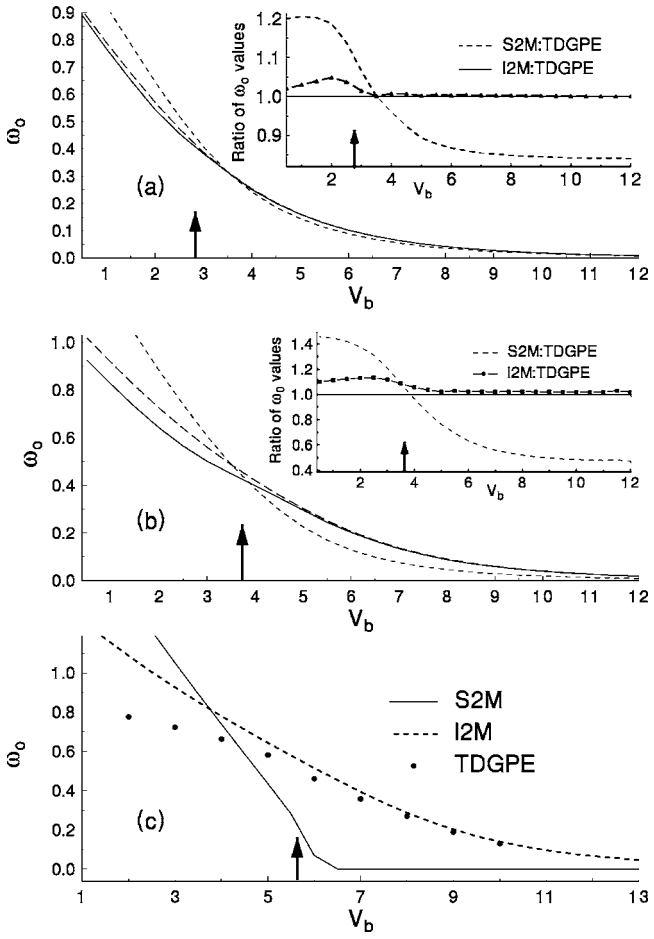

FIG. 3. Comparisons of the oscillation frequencies for small z, ϕ amplitude calculated from the S2M, the I2M, and the TDGP equation, for $gN=1.0$ (a), 3.0 (b), 10.0 (c). The insets in (a) and (b) show ratios of S2M and I2M results to TDGPE results. Vertical arrows denote values of V_B for which $V_b=\beta_+$.

In every 1D case we have considered, $B-2C>0$ and $A+B-C>0$. Numerical results obtained with the I2M and S2M are shown in Fig. 3 in comparison with frequencies obtained with the TDGP equation. For $\bar{g} \ll 1$, all three approaches agree well. For $\bar{g}=1$ and large V_b, the values for ω_0 from the S2M are about 16% less than from the I2M, while for $\bar{g}=3$, the asymptotic difference is about a factor of 2. For larger values of $\bar{g}$ and for large V_b, as illustrated for $\bar{g}=10$ in Fig. 3(c), $\mathcal{K}$ becomes negative, hence ω_{0S} becomes imaginary, and the real part of ω_0 plotted in Fig. 3 is zero. We note also that in view of the factor $(B-2C)^{1/2}$ in ω_{0I}, when $C/B=0.15$, the C term produces a decrease in ω_{0I} by about 15% due to the effect of wave-function overlap in the tunneling integral.

Values of B, $2\mathcal{K}$, and $\Delta\gamma$ for $\bar{g}=10$ and $\sigma_z=1.5$ are shown in Fig. 4. The region where $\mathcal{K}<0$ is clearly indicated. $\beta_\pm$ are the actual eigenvalues, which are calculated with the nonlinear interaction terms included. The quantities $\epsilon_\pm$ have no direct physical meaning, so it is not surprising that they can lead to anomalous results. Note also that the putative regime of validity of two-mode models is to the right of the vertical arrows in Figs. 3 and 4, and that for $\bar{g}=10$, $\mathcal{K}$ is negative over most of this region.

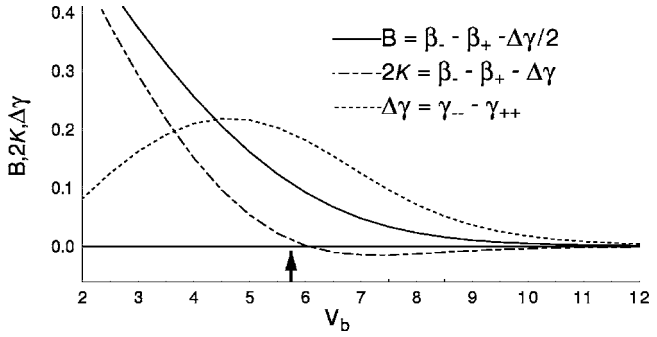

FIG. 4. Values for the parameters B, $2\mathcal{K}$, and $\Delta\gamma=\gamma_{--}-\gamma_{++}$ for $\bar{g}=10$ and values of the barrier height V_b as indicated. Although $\mathcal{K}$ becomes negative for $V_b>6$, B remains positive.

Thus from calculations of the Josephson plasma oscillation frequencies, we conclude that the additional terms derived in the I2M take better account of nonlinear interaction effects and produce better agreement with full TDGPE results. For low atomic numbers and weak interactions, these additional terms are not needed. It is also evident that as interactions increase in magnitude, neither two-mode model reproduces TDGPE results quantitatively. This will lead us to examine multimode models below.

First, however, it will be helpful to take another perspective by looking at results simply from the TDGPE. Figure 5 shows $|\Psi(x)|^2$ and $\phi(x)$ as they evolve over one-half cycle under conditions in which [in (a) and (b)] the phase is nearly constant over each well, and [in (c) and (d)] with a larger $\bar{g}$ interaction parameter such that the phase over each well is not constant at a given time. In the latter case, the phase difference cannot be defined, and any two-mode model fails.

Another derived property is the onset of self-trapping at $\phi=0$, which is usually labeled z_c, the critical value of z. We will discuss this in Sec. II D.

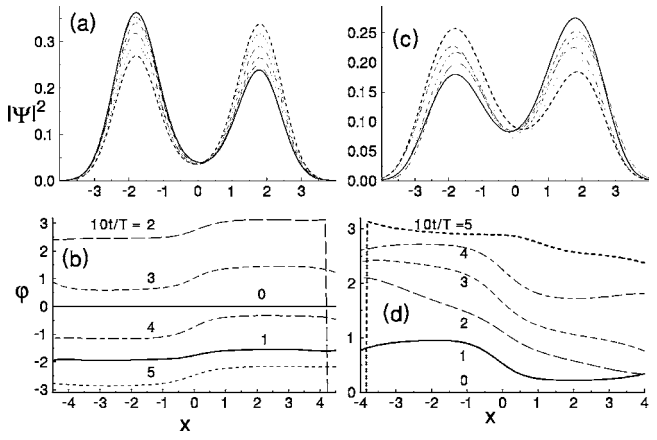

FIG. 5. (a) and (c) Evolution of $|\Psi(x)|^2$ over one-half cycle of tunneling oscillation. (b) and (d) Evolution of phase $\phi(x)$ under the same conditions as in (a) and (c), respectively. The conditions for (a) and (b) are $\bar{g}=2.0$, $V_0=5.0$; for (c) and (d), $\bar{g}=10.0$, $V_b=5.0$; and in each case $\sigma=1.5$. In (a) and (c), the initial function $|\Psi(x)|^2$ is denoted by thick solid lines. In (b) and (d), the initial value of the phase is everywhere zero. In (d) after the initial time, the phase is clearly not uniform over either well because of the strong interactions and low barrier.

C. Multimode approximation

From Fig. 3, we saw that there are deviations in the Josephson plasma frequency ω_0 between even the more exact (I2M) two-mode model and numerical solutions of the TDGPE. These deviations raise the question whether better agreement can be obtained by expanding the set of basis functions beyond simply Φ_+ and Φ_-.

In this section we introduce a generalization of the improved two-mode model. Starting from the TDGP equation

$$i\frac{\partial\psi}{\partial t}=-\frac{1}{2}\frac{\partial^2\psi}{\partial x^2}+V_{\rm ext}\psi+g|\psi|^2\psi \tag{30}$$

we introduce the following ansatz:

$$\psi(x,t)=\sqrt{N}\sum_{k=0}^{N-1}b_k(t)e^{-i\beta_k t}\phi_k(x) \tag{31}$$

where $\phi_k(x)$ satisfy the equations

$$\beta_{2s}\phi_{2s}=-\frac{1}{2}\frac{d^2\phi_{2s}}{dx^2}+V_{\rm ext}\phi_{2s}+\bar{g}|\phi_0|^2\phi_{2s}, \tag{32}$$

$$\beta_{2s+1}\phi_{2s+1}=-\frac{1}{2}\frac{d^2\phi_{2s+1}}{dx^2}+V_{\rm ext}\phi_{2s+1}+\bar{g}|\phi_1|^2\phi_{2s+1}. \tag{33}$$

Thus $\phi_{0,1}=\Phi_\pm$ as defined above, with normalization $\int dx\,\phi_i(x)\phi_j(x)=\delta_{ij}$. Here we are effectively using the virtual excited states of the Gross-Pitaevskii equation rather than Bogoliubov quasiparticle states. Equilibrium thermodynamics is not the goal here. Any orthonormal basis offers an extension of the two-mode model, and the quasiparticle basis is unnecessarily cumbersome for this application. Substituting the ansatz (31) into the GP equation (30) and using equations for $\phi_{2s}(x)$ and $\phi_{2s+1}(x)$ with the orthogonality property, we obtain the following equation for the time-dependent amplitudes $b_r(t)$:

$$i\dot{b}_r=-\sum_j b_{2j}\gamma_{00,2j,r}e^{i(-\beta_{2j}+\beta_r)t}-\sum_j b_{2j+1}\gamma_{11,2j+1,r}e^{i(-\beta_{2j+1}+\beta_r)t}+\sum_{s,n,m}b_n b^* b_s\gamma_{nmsr}e^{i(-\beta_n+\beta_m-\beta_s+\beta_r)}. \tag{34}$$

There are $2J$ equations for real functions $|b_j(t)|$ and $\arg[b_j(t)]$, where J is number of modes. However there is the following constraint: $\Sigma_j|b_j(t)|^2=1$, which is a consequence of the normalization condition for the wave function $\psi(x,t)$. Since also the overall phase is arbitrary, we effectively have $2J-2$ equations for $2J-2$ independent variables. Therefore, we define $b_j(t)=c_j(t)e^{i\alpha_j(t)}$, with $c_j(t)=|b_j(t)|$, and introduce the following variables:

$$\Delta_r=c_0^2-c_r^2,\quad r=1,\ldots,J-1,$$

$$\varphi_r=\alpha_{r-1}-\alpha_r,\quad r=1,\ldots,J-1.$$

It is not difficult to restate Eqs. (34) in terms of the new variables.

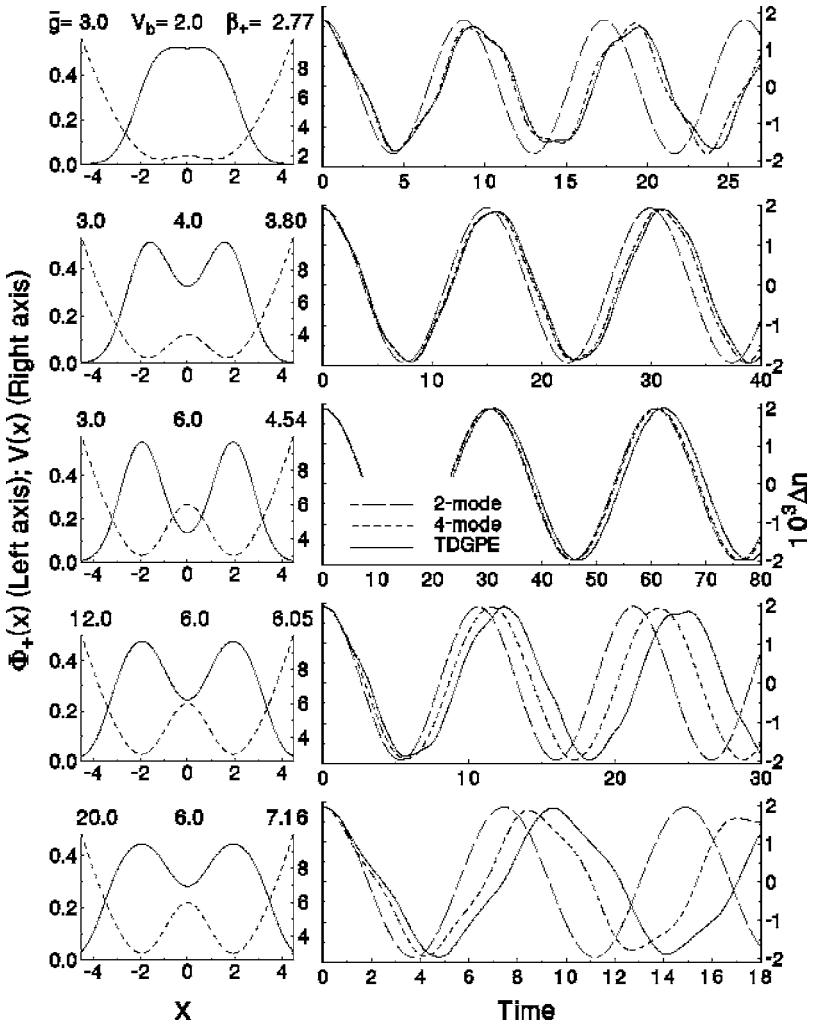

FIG. 6. Left column: The functions $\Phi_+(x)$ and potentials $V(x)$ for conditions indicated above each frame: $\bar{g}, V_b$, with $\sigma_z=1.5$ in each case. The last figure gives the chemical potential β_+. Right column: time evolution of the fractional number difference, Δn, times 10^3 for very small initial imbalance. The three curves are obtained from the I2M model (long dashes), the four-mode model (short dashes), and the TDGPE (solid curve).

As in the case of the I2M, the main ingredients of multimode approximation are parameters γ_{klmn} that can be found numerically from eigenfunctions of the Gross-Pitaevskii operator for the symmetric and antisymmetric "condensates." In making comparisons with two-mode model results and with numerical solutions of the TDGPE, we will use the number difference $\Delta n(t)$ defined in Eq. (10), rather than $z(t)$, which is not defined for the TDGPE. As an initial condition for the TDGPE, we use desired linear combinations of $\Phi_\pm$ [relabeled $\phi_{0,1}$ in Eq. (32)]. In a given experimental situation, the actual initial condition might differ and might need to be modeled more precisely.

What our results show generally is that in circumstances in which the I2M differs significantly from TDGPE, the time evolution curve is not sinusoidal, but is distorted by higher-frequency components. Therefore one cannot easily extract a single frequency, for example, to correct the discrepancies exhibited in Fig. 3. Figure 6 shows the actual time evolution curve for several cases. These curves should be viewed in light of the nominal condition for validity of two-mode models, $\beta_+ < V_b$. As shown in this figure, the two-mode model agrees quite well with the TDGPE curve for $\bar{g}=3.0, V_b=6.0$, for which $\beta_+=4.54$ is less than V_b. For larger $\bar{g}$ or smaller V_b, the two-mode and TDGPE curves differ in both frequency and shape. In each of these cases, results obtained with a four-mode model yield better agreement with the TDGPE curves. It is remarkable that this good agreement appears even for a very low barrier, $V_b=2.0$, for $\bar{g}=3.0$.

In connection with the time variations of Δn shown in Fig. 6, it is pertinent to plot also the ratios of C to B, as an indication of the relative magnitude of C under varying conditions. Figure 7 shows this ratio (left axis) for $V_b=6.0$, as in the lower three cases of Fig. 6. The quantity labeled "$E_{\rm ex}/\Delta\beta$" is the ratio of the second excited state to $\Delta\beta$. As this ratio diminishes, the two-mode model becomes less valid, and this is reflected also in the departure of the time evolution functions in Fig. 6 from sinusoidal shape, and from the TDGPE results. Figure 7(b) will be discussed in connection with the results of 3D calculations.

D. Phase-space dynamics

The evolution of z, ϕ from the coupled equations (22) closely resembles the dynamical evolution phenomena thoroughly discussed in Ref. [10]. We give a brief review to point out the differences arising from use of the I2M.

To visualize the dynamics, it is helpful to view a plot of the Hamiltonian surface $H(z,\phi)$ as shown in Fig. 8 for generic values of A, B, and C. The surface is periodic in ϕ, with minima at $z=0, \phi=2n\pi$ and saddle points or maxima at

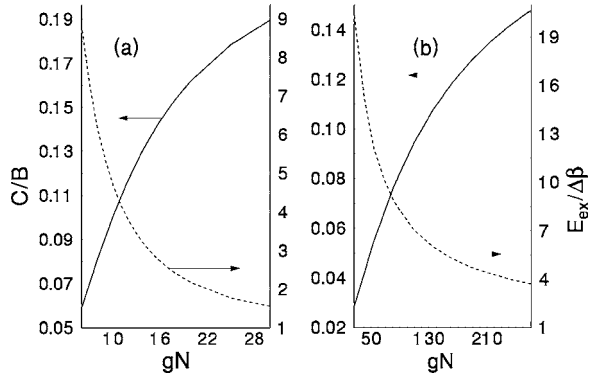

FIG. 7. Ratios of C to B for (a) 1D, with $V_b=6.0$, as in the bottom three parts of Fig. 6; and (b) 3D, for the geometry of the experiments discussed in Sec. III B. The dashed curves and right axes give the ratio of the second to the first excitation energy, which is a measure of the validity of the two-mode approximation. For 3D, we show the ratio of excitation energy to the lowest excited state symmetric in x, y, and z to the excitation energy of the lowest state antisymmetric in z.

$z=0, \phi=(2n+1)\pi$, where n is an integer. Trajectories are horizontal curves (constant H) lying on this surface.

Within either two-mode model, self-trapping occurs for H above H_s, the value of the classical Hamiltonian at the saddle point. Critical values of $z=z_c$ are defined as values of $z(\phi=2n\pi)=z_0$ that give $H(z,\phi)$ equal to H_s. For $|z_0|>z_c$, trajectories will not pass through $z=0$ and z will remain positive or negative. For the I2M, the Hamiltonian given by Eq. (24) gives

$$H_s = H(0,\pi) = B + \frac{C}{2} = H(z_c,0). \tag{35}$$

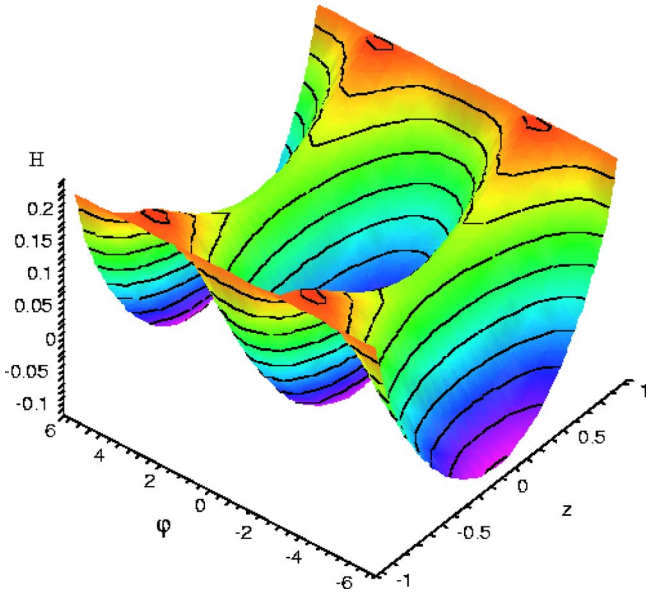

FIG. 8. (Color online) Hamiltonian surface $H(z,\phi)$ for $V_0=4, \sigma=1.5, \bar{g}=1$. Trajectories lie on the surface, following contour lines that represent constant energy levels.

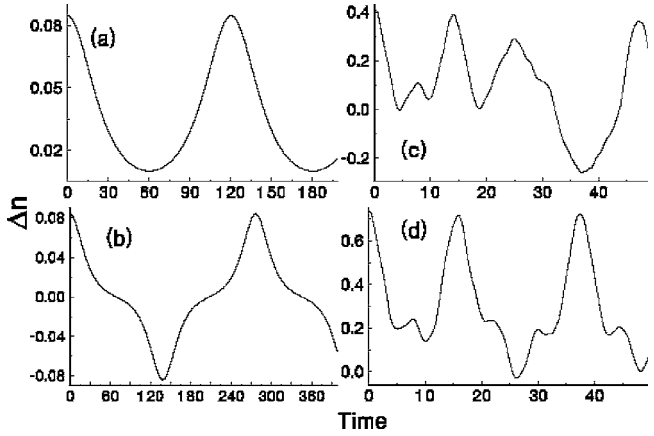

FIG. 9. Temporal evolution of Δn for various cases: (a) $\bar{g}=3.0, V_b=9.0, z_0=\Delta n(0)=0.0846$; (b) $\bar{g}=3.0, V_b=9.0, \Delta n(0)=0.0838$; (c) $\bar{g}=10.0, V_b=5.5, \Delta n(0)=0.411$; (d) $\bar{g}=3.0, V_b=4.0, \Delta n(0)=0.735$.

From this result and Eq. (24), we obtain

$$z_{c,V} = \frac{2}{A-C}[B(A-B-C)]^{1/2}. \tag{36}$$

For the S2M, the Hamiltonian of Eq. (25) yields

$$H_s = H(0,\pi) = 2\mathcal{K} = H(z_c,0), \tag{37}$$

so that

$$z_{c,C} = \frac{2}{U}[2\mathcal{K}(U-2\mathcal{K})]^{1/2}. \tag{38}$$

Here the model breaks down when either $\mathcal{K}<0$ (see Fig. 4) or $U-2\mathcal{K}<0$.

Before presenting results of calculations of z_c, we recognize that as $|z|\approx|\Delta n|$ and $\bar{g}$ increase, as in Fig. 6, higher modes enter. The variation of Δn with time becomes irregular rather than close to sinusoidal, as shown by several plots obtained from calculations with the TDGPE in Fig. 9. Figures 9(a) and 9(b) [differing very slightly in $\Delta n(0)$, but on opposite sides of $\Delta n=z_c$], closely resemble results one would expect from a two-mode model. Figures 9(c) and 9(d) show irregular curves from the TDGPE in a regime where the two-mode model does not apply. In Fig. 9(c), there are oscillations of Δn within the range $\Delta n>0$ before Δn eventually becomes less than 0. Figure 9(d) shows that $\Delta n<0$ is achieved for only a brief duration (between $T=25$ and 29). Neither of these cases can be considered "self-trapping," but they are far removed from symmetric, periodic oscillations. Under such conditions of low barrier and/or strong interactions, it is somewhat arbitrary to make the distinction between self-trapping and not self-trapping.

Nonetheless, we have attempted to establish criteria and apply them consistently so as to compare results from the S2M, I2M, and TDGPE approaches, as shown in Fig. 10. Here, z_c values from Eqs. (36) and (38) have been restated in terms of Δn_c using Eq. (10) in order to compare with

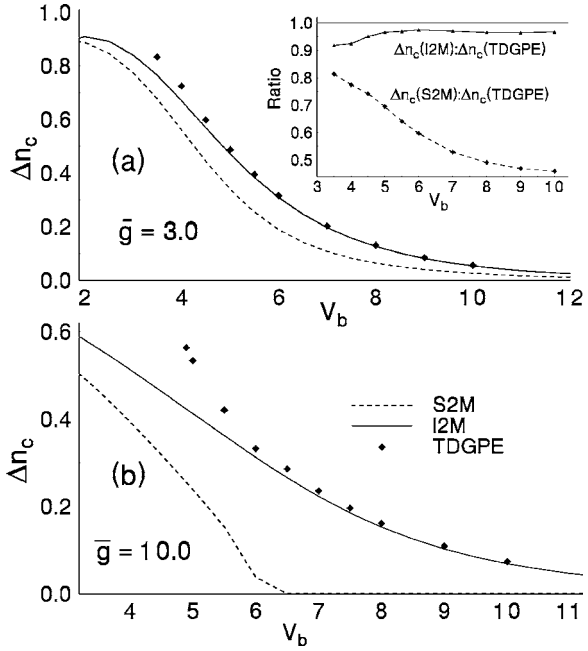

FIG. 10. Values for Δn_c from the S2M, I2M, and TDGPE approaches, for $\bar{g}$= (a) 3.0 and (b) 10.0. The inset in (a) shows the ratio of S2M and I2M values to TDGPE results.

TDGPE results. For both $\bar{g}=3.0$ and 10.0, when V_b is high enough, there is good agreement between I2M and TDGPE results. S2M results are significantly lower for $\bar{g}=3.0$, while for $\bar{g}=10.0$, as in Fig. 3, the fact that $\mathcal{K}$ becomes negative invalidates this approach in this regime of strong interactions.

In the self-trapping regime, maximal and minimal values of $z(t)$ can be obtained by solving the equation $\dot{z}=0$:

$$z = \pm \sqrt{1 - \left[\frac{|B|}{C-A} \pm \sqrt{\left(\frac{B}{C-A}\right)^2 - \frac{2H-A}{C-A}} \right]^2}. \quad (39)$$

Plus or minus signs in front of the square root correspond to different initial conditions for z (positive or negative, respectively). An elegant discussion of dynamics, and separatrices, in phase space is given in Ref. [12] (explicitly for the case $C=0$).

In Ref. [10], it was pointed out that closed trajectories on the surface of H can also occur around maxima on the lines $\phi=(2n+1)\pi$. These are the so-called π-phase modes. For the I2M, the condition for these maxima is that $|B| < |(A+C)|$. The actual values z_π at which these maxima occur can vary drastically from one model to the other.

Even for the case of negligibly small overlap, the momentum $z(t)$ in the I2M differs drastically from the S2M when conditions place these two models on opposite sides of the transition to self-trapping. Far from the neighborhood of the self-trapping transition in $\bar{g}, \sigma, V_0$, the differences are less. We note also that the C term raises both the minimum and the saddle point in $H(z,\phi)$, and changes the shape of the surface because it introduces a term with a periodicity of π rather than 2π. However, no new critical points or minima are introduced for values of $C/B<0.5$, which is outside the regime of validity of two-mode models, as noted in connection with Fig. 7.

E. Second quantization

Previous discussions of quantized versions of the Bose double-well problem [4,9,18] are to first order in the overlap of the wave functions in each well. Using the I2M, there are further possibilities for extending the regime of validity of quantum approaches, which are necessarily based on two-mode models.

The energy functional describing a trapped Bose-Einstein condensate in terms of creation and annihilation operators $\psi(x,t)$, $\psi^\dagger(x,t)$ can be written

$$\hat{H}_2 = \hat{H}_0 + \hat{H}_1, \quad \hat{H}_0 = \int dx \left(-\frac{1}{2}\hat{\psi}^\dagger \nabla^2 \hat{\psi} + \hat{\psi}^\dagger V_{\text{ext}} \hat{\psi} \right),$$

$$\bar{H}_1 = \frac{g}{2} \int dx\, \hat{\psi}^\dagger \hat{\psi}^\dagger \hat{\psi}\hat{\psi}, \quad (40)$$

with the commutator $[\hat{\psi}(x,t), \hat{\psi}^\dagger(x',t)] = \delta(x-x')$.

As above, we will characterize the time evolution in terms of two modes that are predominantly (but not exclusively) located in the left and right wells. However, the derivation is easier when written in terms of the symmetric and antisymmetric functions $\Phi_\pm$ rather than in terms of $\Phi_{1,2}$, because $\langle \Phi_\pm^3 \Phi_\mp \rangle = 0$, whereas $\langle \Phi_{1,2}^3 \Phi_{2,1} \rangle \neq 0$. We therefore write a "mixed basis" expression

$$\hat{\psi} = \frac{1}{\sqrt{2}} \left[\hat{c}_1 (\Phi_+ + \Phi_-) + \hat{c}_2 (\Phi_+ - \Phi_-) \right], \quad (41)$$

in which

$$\hat{c}_{1,2} = \frac{1}{\sqrt{2}} \int dx\, \hat{\psi} (\Phi_+ \pm \Phi_-) \quad (42)$$

are projections of $\hat{\psi}$. $\Phi_\pm$ are solutions to the GP equation as above. In particular,

$$-\frac{1}{2}\nabla^2 \Phi_i + V_{\text{ext}} \Phi_i = \beta_i \Phi_i - gN|\Phi_i|^2 \Phi_i. \quad (43)$$

Also $[\hat{c}_i, \hat{c}_j^\dagger] = \delta_{ij}$.

Substituting Eqs. (41) and (43) into the above equation for H_0, we obtain four terms:

$$\hat{H}_0 = \frac{1}{2} [(\hat{c}_1^\dagger \hat{c}_1 + \hat{c}_2^\dagger \hat{c}_2)(\beta_+ - \gamma_{++} + \beta_- - \gamma_{--}) + (\hat{c}_1^\dagger \hat{c}_2 + \hat{c}_2^\dagger \hat{c}_1)(\beta_+ - \gamma_{++} - \beta_- + \gamma_{--})], \quad (44)$$

Upon substituting Eq. (41) into the above equation for $\bar{H}_1$, we obtain 16 terms, each with products of two creation and two annihilation operators, times integrals of the form

$$(+)^i(-)^j = \frac{g}{2} \int dx (\Phi_+ + \Phi_-)^i (\Phi_+ - \Phi_-)^j. \quad (45)$$

In particular

$$H_1 = \hat{c}_1^\dagger \hat{c}_1^\dagger \hat{c}_1 \hat{c}_1 (+)^4 + \hat{c}_2^\dagger \hat{c}_2^\dagger \hat{c}_2 \hat{c}_2 (-)^4 + (\hat{c}_1^\dagger \hat{c}_1^\dagger \hat{c}_1 \hat{c}_2 + \hat{c}_1^\dagger \hat{c}_1^\dagger \hat{c}_2 \hat{c}_1 + \hat{c}_1^\dagger \hat{c}_2^\dagger \hat{c}_1 \hat{c}_1 + \hat{c}_2^\dagger \hat{c}_1^\dagger \hat{c}_1 \hat{c}_1)(+)^3(-) + (\hat{c}_2^\dagger \hat{c}_1^\dagger \hat{c}_1 \hat{c}_2 + \hat{c}_2^\dagger \hat{c}_1^\dagger \hat{c}_2 \hat{c}_1 + \hat{c}_2^\dagger \hat{c}_2^\dagger \hat{c}_1 \hat{c}_1 + \hat{c}_1^\dagger \hat{c}_2^\dagger \hat{c}_1 \hat{c}_2 + \hat{c}_1^\dagger \hat{c}_2^\dagger \hat{c}_2 \hat{c}_1 + \hat{c}_1^\dagger \hat{c}_1^\dagger \hat{c}_2 \hat{c}_2)(+)^2(-)^2 + (\hat{c}_2^\dagger \hat{c}_2^\dagger \hat{c}_1 \hat{c}_2 + \hat{c}_2^\dagger \hat{c}_2^\dagger \hat{c}_2 \hat{c}_1 + \hat{c}_2^\dagger \hat{c}_1^\dagger \hat{c}_2 \hat{c}_2 + \hat{c}_1^\dagger \hat{c}_2^\dagger \hat{c}_2 \hat{c}_2)(+)(-)^3. \tag{46}$$

In view of definitions given above, we obtain

$$(\pm)^4 = \frac{2U}{N}, \quad (\pm)^3(\mp) = -\frac{\Delta\gamma}{2N}, \quad (+)^2(-)^2 = \frac{2C}{N}. \tag{47}$$

We express $\bar{H}_2$ in terms of the following operators:

$$\hat{N} = \hat{N}_1 + \hat{N}_2 = \hat{c}_1^\dagger \hat{c}_1 + \hat{c}_2^\dagger \hat{c}_2, \quad \hat{J}_x = \frac{1}{2}(\hat{c}_2^\dagger \hat{c}_2 - \hat{c}_1^\dagger \hat{c}_1),$$

$$\hat{J}_y = \frac{i}{2}(\hat{c}_2^\dagger \hat{c}_1 - \hat{c}_1^\dagger \hat{c}_2), \quad \hat{J}_z = \frac{1}{2}(\hat{c}_2^\dagger \hat{c}_1 + \hat{c}_1^\dagger \hat{c}_2), \tag{48}$$

and the Casimir element $\hat{J}^2 = (\hat{N}/2)(\hat{N}/2+1)$, so that

$$[\hat{J}_i, \hat{J}_j] = i\epsilon_{ijk}\hat{J}_k. \tag{49}$$

Then using relations such as

$$(\hat{c}_1^\dagger)^2 \hat{c}_1^2 + (\hat{c}_2^\dagger)^2 \hat{c}_2^2 = \frac{\hat{N}^2}{2} - \hat{N} + 2\hat{J}_x^2, \tag{50}$$

collecting terms, and neglecting constant terms, we obtain

$$\hat{H}_2 = -\hat{J}_z\left(\Delta\beta + \Delta\gamma - \frac{2\Delta\gamma}{N}\right) + \frac{4(A+C)}{N}\hat{J}_x^2 + \frac{8C}{N}\hat{J}_z^2. \tag{51}$$

Since

$$\hat{J}_z^2 = \frac{1}{4}(\hat{c}_2^\dagger \hat{c}_2^\dagger \hat{c}_1 \hat{c}_1 + \hat{c}_1^\dagger \hat{c}_1^\dagger \hat{c}_2 \hat{c}_2) + \frac{1}{2}(1 + \hat{N}_1 \hat{N}_2), \tag{52}$$

the last term contains correlated hopping or two-particle tunneling effects. Quantum equations of motion can be obtained from

$$\dot{\hat{J}}_i = i[\hat{H}, \hat{J}_i]. \tag{53}$$

The above Hamiltonian $\hat{H}_2$ is to be compared with expressions derived previously [4,9,12,15,18,19]. Although a general second-quantized Hamiltonian was written many years ago by nuclear physicists [37] (since known as the Lipkin-Meshkov-Glick model), most applications involve simply the terms in $\hat{J}_z$ and $\hat{J}_x^2$. Using the operators defined above and assuming a symmetric double-well potential, the expression in Ref. [15], for example, can be written

$$\hat{H}_{\text{canon}} = -\mathcal{E}_J \hat{J}_z + \frac{1}{2}K\hat{J}_x^2. \tag{54}$$

The comparison provides the following translation:

$$\mathcal{E}_J = \Delta\beta + \Delta\gamma - \frac{2\Delta\gamma}{N}, \quad K = \frac{8(A+C)}{N}. \tag{55}$$

The regimes defined in Ref. [15] then become (neglecting the $2\Delta\gamma/N$ term)

$$\frac{K}{\mathcal{E}_J} \ll \frac{1}{N} \Rightarrow R \ll 1, \quad R = \frac{8(A+C)}{\Delta\beta + \Delta\gamma} \quad \text{(Rabi)},$$

$$\frac{1}{N} \ll \frac{K}{\mathcal{E}_J} \ll N \Rightarrow 1 \ll R \ll N^2 \quad \text{(Josephson)},$$

$$N \ll \frac{K}{\mathcal{E}_J} \Rightarrow N^2 \ll R \quad \text{(Fock)}. \tag{56}$$

Thus for the second-quantized version as for the first-quantum GP equation version discussed above, we obtain a Hamiltonian with a form similar to those previously derived, but with slightly different parameters, and with extra terms that may be important for large atom-atom interactions. The expectation value $\langle 2\hat{J}_x \rangle$ describes the difference between the number of particles in the two modes, and is therefore an analog of the classical quantities momentum $z(t)$ and number difference $\Delta n(t)$. This connection can be most easily seen in the limit of very small interactions (small $\bar{g}$), which is essentially the Rabi regime as defined in Ref. [15] and above. From numerical results, we find that for $\bar{g} < 10^{-2}$, there are clear tunneling oscillations with frequency $\Delta\beta$ from the first term in $\hat{H}_2$ ($\Delta\gamma \ll \Delta\beta$ here). These oscillations are modulated by effects from the second term (in $\hat{J}_x^2$) in $\hat{H}_2$, which increase with $\bar{g}$. For long enough times, one observes the collapse and revival effects noted in Ref. [4]. For larger values of $\bar{g}$, these structures do not persist. Extensive numerical results of phase-space oscillations are given in Ref. [19], and detailed studies of averages in phase space using the Husimi distribution have been presented in Ref. [18].

III. CALCULATIONS IN 3D

A. General formalism

In comparing with experimental results, the transverse confinement enters. In this study, we consider moderate transverse confinement, not approaching the Tonks-Girardeau regime [38]. We have extended the above methods to 3D as follows. We write the TDGPE first in MKS units, denoted by overbars:

$$i\hbar\frac{\partial\bar{\psi}}{\partial\bar{t}} = \left(-\frac{\hbar^2}{2m}\bar{\nabla}^2 + \frac{m}{2}\sum_i \omega_i^2 \bar{x}_i^2 + V_B + g_{3\text{D}}|\bar{\psi}(\bar{\mathbf{x}},t)|^2\right)\bar{\psi}(\bar{\mathbf{x}},t) \tag{57}$$

where m is the atomic mass, $g_{3\text{D}} = 4\pi\hbar^2 a_{3\text{D}}/m$, $a_{3\text{D}}$ is the 3D scattering length, and $\int d\bar{\mathbf{x}}\,|\bar{\psi}(\bar{\mathbf{x}})|^2 = N$. The external potentials of interest here will include a purely harmonic term as given above, plus a barrier term as a function of z that will be chosen to be Gaussian or proportional to a $\cos^2$ function, as in the experiments of Ref. [24].

We let

$$\omega_x = \omega_y = \eta\omega_z, \tag{58}$$

and scale the coordinates and time as

$$\bar{x}_i = \alpha_i x_i, \quad \alpha_i^2 = \hbar/m\omega_i, \quad \bar{t} = t/\omega_z. \tag{59}$$

Then since

$$\int d\mathbf{x}|\psi(x)|^2 = N = \int d\bar{\mathbf{x}}|\bar{\psi}(\bar{\mathbf{x}})|^2 = \alpha_x\alpha_y\alpha_z \int d\mathbf{x}|\bar{\psi}(\mathbf{x})|^2, \tag{60}$$

$\bar{\psi}=(\alpha_x\alpha_y\alpha_z)^{-1/2}\psi$, and Eq. (57) becomes

$$i\frac{\partial\psi(x,y,z,t)}{\partial t} = \mathcal{H}(\lambda,\psi)\psi(x,y,z,t),$$

$$\mathcal{H}(\lambda,\psi) = -\frac{\eta}{2}\left(\frac{\partial^2}{\partial x^2}+\frac{\partial^2}{\partial y^2}\right) - \frac{1}{2}\frac{\partial^2}{\partial z^2} + \frac{\eta}{2}(x^2+y^2) + \frac{z^2}{2} + V_B + 4\pi\eta\left(\frac{a_{3D}}{\alpha_z}\right)|\psi(x,y,z,t)|^2 \tag{61}$$

where λ represents the arguments η, V_B, N, a_{3D}, and α_z.

An ansatz analogous to Eq. (2) can now be introduced:

$$\psi(\mathbf{x},t) = \sqrt{N}[\psi_1(t)\Phi_1(\mathbf{x}) + \psi_2(t)\Phi_2(\mathbf{x})], \tag{62}$$

$$\Phi_{1,2}(\mathbf{x}) = \frac{\Phi_+(\mathbf{x}) \pm \Phi_-(\mathbf{x})}{\sqrt{2}}, \tag{63}$$

where

$$\Phi_\pm(x,y,z) = \pm\Phi_\pm(x,y,-z), \quad \int dx\,dy\,dz\,\Phi_\pm^2 = 1. \tag{64}$$

The stationary GP equations take the form

$$\beta_\pm\Phi_\pm(x,y,z) = \mathcal{H}(\lambda,\Phi_\pm)\Phi_\pm(x,y,z). \tag{65}$$

Because the transverse wave function is very nearly Gaussian, some authors have simply assumed a Gaussian, possibly with a z-dependent width, and obtained modified equations [39,41] for what we have called $\psi_1(z)$. Because we wanted to consider cases where the Gaussian form may not be valid, we used general 3D algorithms. Initial $\Phi_\pm$ wave functions were obtained by diagonalizing the DVR Hamiltonian [36] using sparse matrix techniques [42], which made calculations with more than 120 000 mesh points possible in minutes on a PC. To calculate the time evolution, the split-operator method [43] with fast Fourier transform [44] was used, requiring an hour or more of $\approx$2 GHz CPU time, in view of the small time steps required.

From the $\Phi_\pm$ functions calculated from the 3D time-independent Gross-Pitaevskii equation, one can also obtain the parameters $\beta_\pm$, $\gamma_{i,j}$, A, B, and C as in Sec. II, to provide a two-mode representation of tunneling oscillations in 3D. In translating results from 1D to 3D for $g_{1D}=g_{3D}=4\pi\eta a_{3D}/\alpha_z$, we find that, in the limit of weak interactions and $\eta\gg 1$, the γ_{ij} functions for 3D are a factor of 2π smaller than the corresponding 1D γ_{ij} functions. The explanation

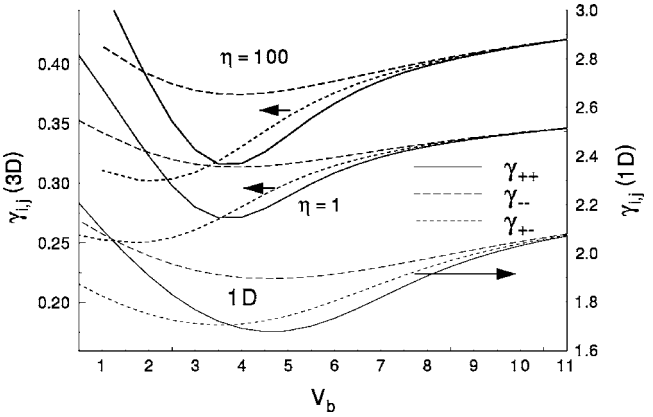

FIG. 11. Values for γ_{ij}, $i,j=+,-$, from 3D calculations with $\eta=1$ and 100 (left axis), as compared with a 1D calculation (right axis). Solid lines denote γ_{++}, short dashes γ_{+-}, and longer dashes γ_{--}. For 3D, the γ_{ij} are approximately 2π larger than for 1D.

touches on the basic properties of tight transverse confinement.

If the transverse confinement is symmetric in x and y and is tight enough, the 3D wave function $\Phi_+(x,y,z)$ can be factored into a function of z and a function of $\rho=\sqrt{(x^2+y^2)}$. Then if also the interactions are weak enough, the ρ function will be a Gaussian:

$$\Phi_+(x,y,z) = \Phi_+(\rho,z)e^{-\rho^2/2}\phi_1(z). \tag{66}$$

The normalization condition is

$$1 = \int dx\,dy\,dz\,\Phi_+(x,y,z)^2 = 2\pi\int d\rho\,\rho e^{-\rho^2}\int dz\,\phi_1(z)^2 = \pi\int dz\,\phi_1(z)^2. \tag{67}$$

Under the above conditions, and if $g_{1D}=g_{3D}$, then to within a constant of proportionality, $\phi_1(z)$ will also be a solution of the 1D problem: $\phi_1(z)\propto\Phi_+^{1D}(z)$. For the 1D problem, $\int dz|\Phi_+^{1D}(z)|^2=1$, so from the different normalizations, we see that, under all the above stated conditions,

$$\phi_1(z) = \frac{1}{\sqrt{\pi}}\Phi_+^{1D}(z). \tag{68}$$

The 3D version of γ_{++} becomes

$$\gamma_{++}^{3D} = \int dx\,dy\,dz|\Phi_+^{3D}|^4 = 2\pi\int\rho\,d\rho\,e^{-2\rho^2}\int dz\,\phi_1(z)^4 = 2\pi\frac{1}{4}\frac{\gamma_{++}^{1D}}{\pi^2} = \frac{\gamma_{++}^{1D}}{2\pi}. \tag{69}$$

Similar relations hold also for γ_{--}^{3D} and γ_{+-}^{3D}. For larger interactions, the ρ dependence is not exactly Gaussian, the functions $\Phi_\pm^{3D}$ no longer factorize, and the parameters γ_{ij}^{3D} deviate from the above relations. Figure 11 shows plots of γ_{++}, γ_{--}, and γ_{+-} from 3D calculations with $\eta=1$ and 100, as compared with 1D results. For $\eta=100$, the wave function is more concentrated than for $\eta=1$, so the values for γ_{ij} are slightly

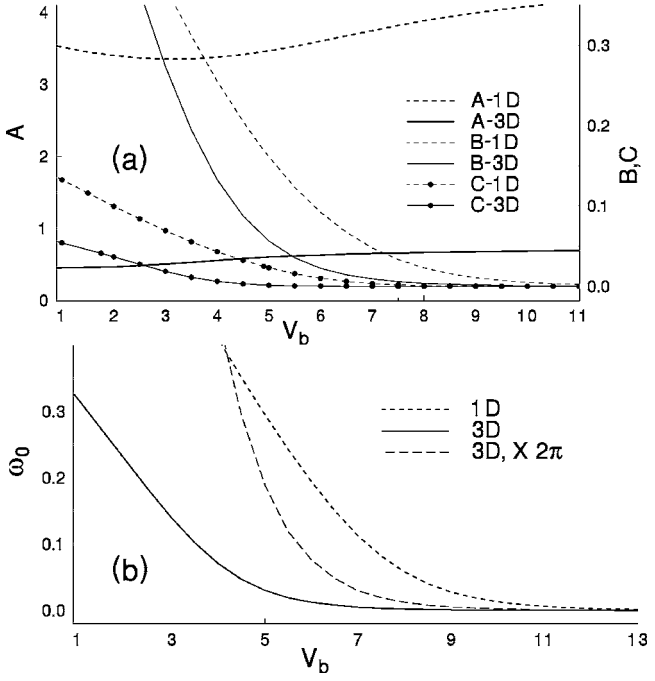

FIG. 12. (a) A comparison of calculated values for the parameters A, B, and C for 1D and for 3D, for $\eta=1$ and $\bar{g}=10$. (b) A comparison of Josephson plasma oscillation frequencies ω_0 for 1D and 3D, also for $\eta=1$ and $\bar{g}=10$.

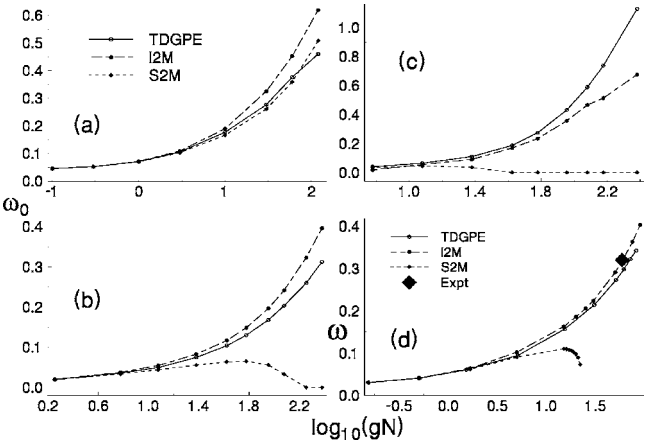

FIG. 13. Josephson plasma oscillation frequencies calculated from the TDGPE and from the I2M and S2M, using Eq. (29) and the $\beta_\pm$, $\epsilon_\pm$, and $\gamma_\pm$ parameters obtained from the 3D wave functions, $\Phi_\pm$. For (a)–(c), Gaussian barriers were used, as in all the 1D calculations. For (d), a $\cos^2$ function was used to reproduce the barrier in Ref. [24]. Other parameters were (a) $\eta=1.0$; $V_b=5.0$; (b) $\eta=1.0, V_b=8.0$; (c) $\eta=100, V_b=8.0$; (d) corresponding closely to the experiments in Ref. [24] (see text), $\nu_x=66$ Hz, $\nu_y=90$ Hz, $\nu_z=78$ Hz, barrier $V_b=5.28\,\hbar\omega_z$ times the $\cos^2$ function given in the text. The values plotted are for $z_0=0.28$ as in the experiments, rather than for the limiting case of small z, ϕ and hence are labeled ω rather than ω_0.

larger. Each is 5–6 times smaller than for the 3D case. Otherwise the dependences on V_b are very similar.

There are other differences between 3D and 1D properties. The difference energy $\Delta\beta$ and hence also the parameter B decrease more rapidly as a function of barrier height. Figure 12 compares the parameters A, B, and C in 3D ($\eta=1$) and in 1D, for the case $\bar{g}=10$. Evidently, finite transverse confinement decreases the difference between the symmetric and antisymmetric condensate energies. The differences are much the same for $\eta=100$ as for $\eta=1$. Also for $\eta=1$, $\bar{g}=10$, Fig. 12(b) shows that the plasma oscillation frequency in the limit of small z, ϕ, for barrier height $V_b>5$, is even less than a factor of 2π smaller in 3D than in 1D. This statement has been found to be true for $\eta=1$ and 100, and $\bar{g}$ up to 10.

We conclude that two-mode models tend to be even more valid in 3D than in 1D.

Linear combinations of $\Phi_\pm$ functions provide the initial condition for the TDGPE, for which we use the split operator approach with fast Fourier transform [43,44]. To be able to compare TDGPE results with Eq. (29), we use a very small initial imbalance ($z_0=0.002$) for the TDGPE calculations. For the two-mode models, parameters are obtained from wave functions calculated with the time-independent 3D GP equation, as for 1D results above. The results for ω_0 are shown in Figs. 13(a)–13(c) [Fig. 13(d) pertains to the experiments of Ref. [24] as discussed below]. The plasma oscillation frequency obtained from the TDGPE increases rapidly beyond $\bar{g}=gN\approx 3$. The two-mode model results match the TDGPE results well for $\bar{g}<1$. Figure 13(a), for Gaussian barrier of height $V_b=5\hbar\omega_z$, shows good agreement for both the I2M and S2M with TDGPE results, up to $\bar{g}=100$. On the other hand, when the barrier height is raised to $8\hbar\omega_z$, the S2M fails for $\bar{g}>30$, for both $\eta=1$ (b) and 100 (c). For the latter, the I2M result begins to deviate significantly from the TDGPE value around $\bar{g}=100$. The failure of the S2M here is analogous to the situation shown in Fig. 3, and occurs because $\mathcal{K}$ becomes negative.

B. Comparison with recent experiments

Very recently, the first quantitative experimental observations of oscillations of Bose condensates in a double-well potential have been performed [24]. The harmonic confinement was created by overlapping tightly focused Gaussian laser beams. The harmonic frequencies were 66, 90, and 78 Hz in what we will call the x, y, and z directions. To produce the double well, an optical standing wave from two beams of wavelength 811 nm at an angle of 9° were added, producing a barrier of the form $V_b\cos(z\pi/w)^2$, with $V_b=413(20)$ Hz, and $w=5.20(20)$ μm. 1150 ^{87}Rb atoms were loaded into this trap. We have modeled this experimental configuration and find the effective value of $gN=58.8$ from Eq. (61), which corresponds to $\bar{g}\approx 10$ in 1D simulations.

The reported experimental period of oscillation for $z_0=0.28(6)$ was 40(2) ms [24], which corresponds to the value indicated by the large diamond in Fig. 13(d). We obtain values very close to this observed tunneling frequency with both the I2M and TDGPE by using a value for $a_{3D}=100a_0$ (where a_0 is the Bohr radius) [45]. For this initial value of z_0, (although not for very small values of z_0), self-trapping occurs with the S2M, when based on solutions of the Gross-Pitaevskii equation. The calculated S2M frequency drops rapidly before this point, as shown in Fig. 13(d).

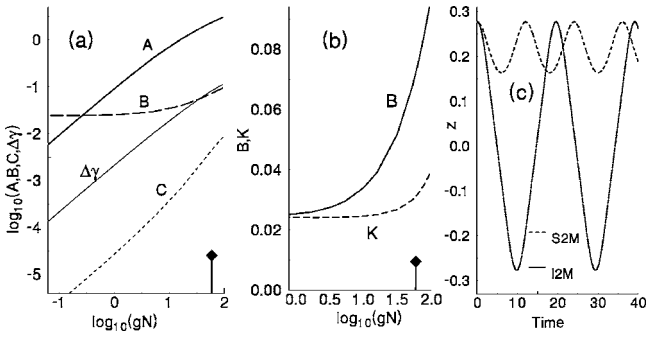

FIG. 14. (a) For the geometry of the experiments in Ref. [24], this plot shows values of A, B, C, and $\Delta\gamma$ vs gN on a log-log scale. The value of gN corresponding to the experiments is indicated with a diamond-headed arrow. (b) A plot of B and $2\mathcal{K}$ on a linear scale shows almost a factor of 3 difference at the experimental value of gN. (c) Because the effective tunneling parameter is greater, the I2M gives oscillations with $\langle z\rangle$, while the S2M gives self-trapping oscillations of smaller amplitude.

To understand this behavior better and to compare the conditions of the experiment [24] with the discussion for 1D above, we show in Fig. 14 a plot of the parameters A, B, C, and $\Delta\gamma$, analogous to Fig. 2 for conditions of the experiment, but with variable atomic number. Figure 14(b) shows values for B and $\mathcal{K}$, the tunneling parameters in the I2M and S2M, respectively, on a linear scale. Because interactions are expressed explicitly in B, this produces approximately three times the tunneling rate as $\mathcal{K}$. Therefore, as shown in Fig. 14(c), there are indeed tunneling oscillations with the I2M, but self-trapping oscillations with the S2M.

This correlates with our earlier statement that the major difference between the two models is in the magnitude of the tunneling parameters. Figure 15 shows the effect of another feature of the I2M, namely, the variation of the tunneling parameter over the oscillation period. In Fig. 15, the temporal variation of z is as shown in Fig. 14(c). When z is maximally positive, the tunneling rate from left to right, namely, $\mathcal{K}_1$, is largest, while when z is maximally negative, $\mathcal{K}_2$ reaches its maximum value. The maximum values are only about 15% larger than the minimum values, so this is not as large an effect as the $B-\mathcal{K}$ difference shown in Fig. 14(b). It is interesting to note that when $z_0=0.40$ where the system was observed to be in the self-trapping regime, the effective tunneling parameters for the atoms in the left and right sides differ also by about 15%, as shown in Fig. 15(b).

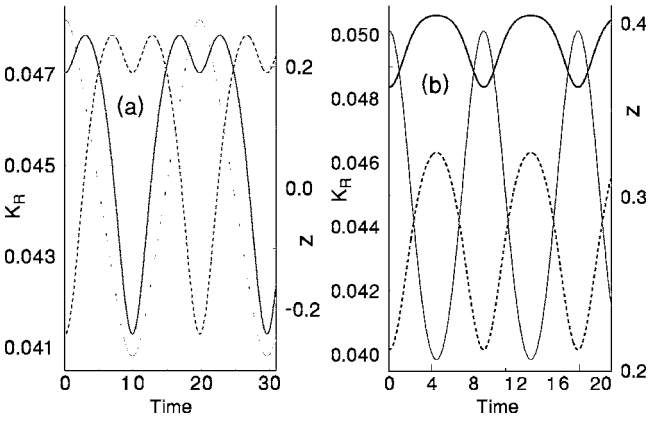

FIG. 15. These plots show variations of the real parts, $\mathcal{K}_{R1}$, and $\mathcal{K}_{R2}$ (heavier solid and dashed lines, left axes) of the effective tunneling parameters, for atoms in the left and right wells, respectively, during oscillations. The lighter solid lines and right axes show the time variation of z. For (a), $z_0=0.24$, for which left-to-right oscillations occur, while for (b) $z_0=0.40$, and there are self-trapping oscillations. In the latter case the tunneling parameter for the well with more atoms is always larger than that for the other well.

The relative importance of the parameter C under the conditions of the experiments, but with varying atom number, is shown in Fig. 7(b). For the experiments discussed here, gN was equal to ≈ 56, so $C/B\approx 0.04$. In more recent work [40], the atom number, and hence C, has been larger. We conclude also, as long as the temperature is sufficiently low the aspect ratio is not important, as indicated in Figs. 13(a)–13(c). Results for $\eta=100$ and 1 are very similar, although the relatively large value of the nonlinear term is important in determining the validity of two-mode models.

Using the TDGPE, we have calculated a value of $z_c=0.39$ for the stated conditions of these experiments, which is consistent with the observed oscillations at $z_0=0.28(6)$ and self-trapping for $z(0)=0.62(6)$, but lower than the value of $z_c=0.50(5)$ quoted in Ref. [24]. See Figs. 14 and 15. In this paper, the authors performed calculations with the transverse Gaussian model of Ref. [39] and obtained good agreement with experimental observations. Our contribution is simply to show that a two-mode model, with parameters from GP eigenfunctions, also comes quite close to reproducing the experimental observations.

The other experiments that helped to motivate this study were performed by Peil *et al.* with ^{87}Rb atoms in a "pattern-loaded" optical lattice. The atoms were first loaded into a coarse lattice from Bragg-diffracted laser beams, and then a finer lattice was turned on, such that every third lattice site was occupied [25]. We are presently working to develop a modification of the present approach to deal with such phenomena in a periodic lattice.

IV. CONCLUSIONS

Two-mode models are useful wherever they might apply, and in particular, they have yielded some compelling results for the problem of Bose-Einstein condensates in a double-well potential. In this work, our goal has been to extend the validity of two-mode models to regimes of larger atom-atom interactions. Our derivation of equations, starting with the Gross-Pitaevskii equation and symmetric and antisymmetric condensate functions, leads to an expression for the tunneling coupling energy that includes the nonlinear interaction. This has commonly been neglected in previous discussions, although given previously by Giovanazzi *et al.* [13]. On the basis of numerical examples for various conditions, we establish that inclusion of such an interaction term explicitly in the tunneling coupling energy is the most important step to deal with larger nonlinear interaction effects. This term also leads to a temporal variation of tunneling as the wave functions expand or contract with changing atom number on either side.

A smaller effect, also arising from the nonlinear interaction, is expressed by a term in the phase-space Hamiltonian proportional to $C\cos 2\phi$. This term leads to a reduction of tunneling when the wave functions in the two wells overlap and interact. Since the term is proportional to the nonlinear interaction, we have labeled C the interaction tunneling parameter. When the I2M is subject to second quantization, this term leads to correlated hopping. This effect is significant only near the limit of the regime of validity of two-mode models, when the value of the chemical potential is close to the barrier height.

Results for oscillation frequencies and self-trapping obtained with the improved two-mode model agree with TDGPE results up to larger values of the nonlinear interaction. For small values of the nonlinear interaction term and moderate potential barriers, all the models agree nicely.

In particular, we show from calculations in 3D that the I2M produces agreement with experimental oscillation frequencies [24], whereas the standard two-mode model, with parameters obtained from the GP equation, produces self-trapping rather than oscillations between the wells. The primary effect is the difference of the mean tunneling energy.

Finally, we note that here we have not considered damping effects on oscillations in the double well due to thermal excitations, as considered in Refs. [6,46,47].

ACKNOWLEDGMENTS

We gratefully acknowledge support from NSF Grant No. PHY0354211, and from the ONR. We are especially indebted to M. Oberthaler for sending a copy of Ref. [24] before publication. Communications with M. Olshanii, V. Dunjko, H. T. C. Stoof, V. Korepin, and D. Averin have been valuable in preparing this paper. In addition, we thank A. Muradyan for a critical reading of the manuscript.

[1] B. D. Josephson, Phys. Lett. **1**, 251 (1962).
[2] J. Javanainen, Phys. Rev. Lett. **57**, 3164 (1986).
[3] M. W. Jack, M. J. Collett, and D. F. Walls, Phys. Rev. A **54**, R4625 (1996).
[4] G. J. Milburn, J. Corney, E. M. Wright, and D. F. Walls, Phys. Rev. A **55**, 4318 (1997).
[5] A. Smerzi, S. Fantoni, S. Giovanazzi, and S. R. Shenoy, Phys. Rev. Lett. **79**, 4950 (1997).
[6] J. I. Cirac, M. Lewenstein, K. Molmer, and P. Zoller, Phys. Rev. A **57**, 1208 (1998).
[7] M. J. Steel and M. J. Collett, Phys. Rev. A **57**, 2920 (1998).
[8] R. W. Spekkens and J. E. Sipe, Phys. Rev. A **59**, 3868 (1999).
[9] J. Javanainen and M. Yu. Ivanov, Phys. Rev. A **60**, 2351 (1999).
[10] S. Raghavan, A. Smerzi, S. Fantoni, and S. R. Shenoy, Phys. Rev. A **59**, 620 (1999).
[11] E. A. Ostrovskaya, Y. S. Kivshar, M. Lisak, B. Hall, F. Cattani, and D. Anderson, Phys. Rev. A **61**, 031601(R) (2000).
[12] R. Franzosi, V. Penna, and R. Zecchina, Int. J. Mod. Phys. B **14**, 943 (2000).
[13] S. Giovanazzi, A. Smerzi, and S. Fantoni, Phys. Rev. Lett. **84**, 4521 (2000).
[14] G.-S. Paraoanu, S. Kohler, F. Sols, and A. J. Leggett, J. Phys. B **34**, 4689 (2001).
[15] A. J. Leggett, Rev. Mod. Phys. **73**, 307 (2001).
[16] J. R. Anglin, P. Drummond, and A. Smerzi, Phys. Rev. A **64**, 063605 (2001).
[17] K. W. Mahmud, J. N. Kutz, and W. P. Reinhardt, Phys. Rev. A **66**, 063607 (2002).
[18] K. W. Mahmud, H. Perry, and W. P. Reinhardt, Phys. Rev. A **71**, 023615 (2005).
[19] A. P. Tonel, J. Links, and A. Foerster, e-print quant-ph/0408161.
[20] L. Pezzé, A. Smerzi, G. P. Berman, A. R. Bishop, and K. A. Collins, New J. Phys. **7**, 85 (2005).
[21] D. V. Averin, A. B. Zorin, and K. K. Likharev, Zh. Eksp. Teor. Fiz. **88**, 692 (1985) [Sov. Phys. JETP **61**, 407 (1985)].
[22] M. R. Andrews, C. G. Townsend, H. -J. Miesner, D. S. Durfee, D. M. Kurn, and W. Ketterle, Science **175**, 637 (1997).
[23] F. S. Cataliotti, S. Burger, C. Fort, P. Maddaloni, F. Minardi, A. Trombettoni, A. Smerzi, and M. Inguscio, Science **293**, 843 (2001).
[24] M. Albiez, R. Gati, J. Fölling, S. Hunsmann, M. Cristiani, and M. K. Oberthaler, Phys. Rev. Lett. **95**, 010402 (2005).
[25] S. Peil, J. V. Porto, B. L. Tolra, J. M. Obrecht, B. E. King, M. Subbotin, S. L. Rolston, and W. D. Phillips, Phys. Rev. A **67**, 051603(R) (2003).
[26] H. Ott, J. Fortágh, S. Kraft, A. Günther, D. Komma, and C. Zimmermann, Phys. Rev. Lett. **91**, 040402 (2003).
[27] J. Williams *et al.*, Phys. Rev. A **59**, R31 (1999).
[28] J. Hu and J. Yin, J. Opt. Soc. Am. B **19**, 2844 (2002).
[29] P. Hommelhoff, W. Hänsel, T. Steinmetz, T. W. Hänsch, and J. Reichel, New J. Phys. **7**, 3 (2005).
[30] D. Jaksch, C. Bruder, J. I. Cirac, C. W. Gardiner, and P. Zoller, Phys. Rev. Lett. **81**, 3108 (1998).
[31] M. P. A. Fisher, P. B. Weichman, G. Grinstein, and D. S. Fisher, Phys. Rev. B **40**, 546 (1989).
[32] A. Trombettoni and A. Smerzi, J. Phys. B **34**, 4711 (2001).
[33] A.-M. Rey, P. B. Blakie, and C. W. Clark, Phys. Rev. A **67**, 053610 (2003).
[34] D. Ananikian and T. Bergeman, Bull. Am. Phys. Soc. **49**, 78 (2004).
[35] Z. Basic and J. C. Light, J. Chem. Phys. **85**, 4594 (1986).
[36] D. T. Colbert and W. H. Miller, J. Chem. Phys. **96**, 1982 (1992).
[37] H. J. Lipkin, N. Meshkov, and A. J. Glick, Nucl. Phys. **62**, 188 (1964). We thank Julien Vidal for pointing out this paper to us.
[38] M. Olshanii, Phys. Rev. Lett. **81**, 938 (1998).
[39] L. Salasnich, A. Parola, and L. Reatto, Phys. Rev. A **65**, 043614 (2002).
[40] R. Gati and M. Oberthaler (private communication).
[41] K. K. Das, Phys. Rev. A **66**, 053612 (2002).
[42] C. W. Murray, S. C. Racine, and E. R. Davidson, J. Comput. Phys. **103**, 382 (1992); E. R. Davidson, Comput. Phys. **7**, 519

(1993).
[43] M. A. Feit, J. A. Fleck, and A. Steiger, J. Comput. Phys. **47**, 412 (1982).
[44] J. W. Cooley and J. W. Tukey, Math. Comput. **19**, 297 (1965).
[45] E. G. M. van Kempen, S. J. J. M. F. Kokkelmans, D. J. Heinzen, and B. J. Verhaar, Phys. Rev. Lett. **88**, 093201 (2002).
[46] I. Marino, S. Raghavan, S. Fantoni, S. R. Shenoy, and A. Smerzi, Phys. Rev. A **60**, 487 (1999).
[47] L. Pitaevskii and S. Stringari, Phys. Rev. Lett. **87**, 180402 (2001).